Friction **12**(3): 510–521 (2024)
https://doi.org/10.1007/s40544-023-0779-x
ISSN 2223-7690
CN 10-1237/TH
RESEARCH ARTICLE

Decohesion of graphene from a uniaxially-stretched substrate: Failure analysis of a frictional adhesive interface

Bo PENG[1], Chaochen XU[1], Qingao WANG[1], Pei ZHAO[3,4], Xiqiao FENG[1,2], Qunyang LI[1,2,*]

[1] *AML, Department of Engineering Mechanics, Tsinghua University, Beijing 100084, China*

[2] *State Key Laboratory of Tribology in Advanced Equipment, Tsinghua University, Beijing 100084, China*

[3] *Center for X-Mechanics and Institute of Applied Mechanics, Zhejiang University, Hangzhou 310027, China*

[4] *State Key Laboratory of Fluid Power and Mechatronic Systems, Zhejiang University, Hangzhou 310027, China*

Received: 12 February 2023 / Revised: 12 March 2023 / Accepted: 09 May 2023

Abstract: Composite structures consisting of two-dimensional (2D) materials deposited on elastic substrates have a wide range of potential applications in flexible electronics. For such devices, robust 2D film/substrate interfacial adhesion is essential for their reliable performance when subjected to external thermal and mechanical loads. To better understand the strength and failure behavior of the 2D film/substrate interfaces, two types of graphene/polymer samples with distinct interfacial adhesion properties are fabricated and tested by uniaxially stretching the substrates. Depending on the interfacial adhesion, two drastically different debonding rates are observed, i.e., rapid snap-through debonding and more progressive crack propagation. Motivated by the experimental observation, we propose an improved shear-lag model with a trapezoidal-shaped cohesive zone to derive an analytical solution for the decohesion behavior. The theoretical model reveals that the decohesion behavior of the frictional adhesive interface is governed by three dimensionless parameters. Particularly, the dimensionless length of the film essentially determines the decohesion rate; while the other two parameters affect the critical substrate strain to initiate debonding. By fitting the experimental data with the theoretical model, the intrinsic adhesion properties of the two samples are obtained with physically meaningful values. This work offers an analytical solution to describing the decohesion behavior of general thin film/substrate systems with a frictional adhesive interface, which is beneficial for characterizing and optimizing the mechanical properties of various thin film/polymer devices.

Keywords: film/substrate systems; adhesion; frictional sliding; interface decohesion; cohesive-zone model

1 Introduction

Owing to their unique electrical and photoelectric properties as well as out-standing mechanical strength [1], two-dimensional (2D) materials have a wide range of potential applications in flexible devices [2–4]. For such applications, 2D materials are often attached to flexible substrates, e.g., polyethylene terephthalate (PET), polymethyl methacrylate (PMMA), or polydimethylsiloxane (PDMS) [5–10]. During active operations of these devices, the flexible substrates are commonly subjected to various thermal and mechanical loading. Deformation of the substrates will be transmitted to the upper 2D materials through the adhesive interface. However, as the in-plane stiffness of the 2D material is typically much higher than that of the flexible substrates, the large difference in deformability would lead to significant shearing along the interface. When the shear stress exceeds the interfacial strength, the adhesive interface will be damaged leading to debonding of the 2D film from the substrate causing failure of the devices. Therefore,

* Corresponding author: Qunyang LI, E-mail: qunyang@tsinghua.edu.cn

understanding the decohesion behavior of adhesive interfaces under stretch-induced shearing is crucial for reliable and robust performance of these 2D film/substrate flexible devices.

To better understand the mechanical behavior of 2D film/substrate interfaces, the classic shear-lag model, a mechanics model that is generally used for analyzing the interfacial interaction of thin film/substrate systems [11], has been adopted to correlate the 2D film strain with the substrate deformation [12–14]. In the shear-lag model, a cohesive zone model (CZM) defining the relationship between the interfacial shear stress and the slip distance is typically used to describe the adhesive interaction of the interface. In order to study the deformation behavior of graphene films on stretched PET substrates, Jiang et al. [12] used a simplified CZM, consisting of a linear strengthening segment and a constant shear stress after a critical slip distance, to theoretically derive the strain distribution of the film. Meanwhile, Guo and Zhu [13] performed a shear-lag analysis with a bilinear CZM, i.e., a linearly strengthening stage followed by a linearly softening stage, and obtained the critical substrate strain for interface debonding. Later, a three-stage CZM, which adds a constant frictional shear stress segment to the bilinear CZM, was proposed by Dai et al. [14] to predict the mechanical properties of graphene/PMMA systems. It is noted that the existing works [12–14] primarily focus on the strain distribution of the film or the shear stress distribution of the interface before interface debonding to interpret the experiments. For example, by fitting the strain distribution of graphene on polymer substrates, one could extract the shear strength of the graphene/PET interfaces [12, 13] and graphene/PMMA interfaces [14]. However, as the applied substrate strains in the experiments were not large enough to initiate interface debonding [12–14], they could not extract the interface decohesion toughness and the full evolution process of the interfacial failure/debonding was not explored either. However, according to a recent work by Cui et al. [15], when the substrate was highly loaded, full debonding would occur along the adhesive interface and cause catastrophic failure of the devices. Therefore, it is of great significance to better understand the full decohesion behavior of the 2D thin film/substrate systems, such as the critical substrate strain to initiate debonding and the debonding rate of the interface.

In this work, the whole interfacial failure process, including both the frictional sliding stage and the full debonding stage, is examined by stretching the substrate to a large extent. Different decohesion behaviors of the adhesive interface with distinct debonding rates are observed experimentally and the underlying mechanism is revealed by an improved theoretical model. More specifically, graphene films are deposited on PDMS substrates with different properties of adhesive interface and the decohesion behaviors are examined by uniaxially stretching the substrates. Depending on the characteristics of the adhesive interface, two distinct types of decohesion processes are observed: rapid debonding and progressive crack propagation. Motivated by the experimental observations, we propose an improved decohesion model to describe the failure behavior of the interfaces. Our model shows that the decohesion is governed by three key dimensionless parameters, i.e., $\bar{L}$, λ, and ε_0. Particularly, $\bar{L}$, representing the dimensionless length of the bonded film, essentially determines the decohesion mode/rate, while the latter two parameters, λ and ε_0, primarily affect the critical substrate strain to initiate debonding. By choosing proper interfacial parameters, the distinct failure behavior observed in our experiment can be well reproduced by our theoretical model with good consistency.

2 Experimental observations: Decohesion with drastically different rates

In this work, two kinds of graphene/substrate samples were fabricated to explore the interface decohesion behavior when the substrate was uniaxially stretched. One was the graphene/PDMS (Gr/PDMS) sample, where the graphene film was directly transferred to the top surface of the PDMS substrate. The other was the graphene/formvar–PDMS (Gr/Fo-PDMS) sample, where an intermediate formvar layer (Tokyo Chemical Industry Company) was dip-coated on the surface of the PDMS substrate to enhance the interfacial adhesion. In both cases, commercially available monolayer polycrystalline graphene films synthesized on copper

foil using chemical vapor deposition (Vigon Technology) were used and they were cut to a size of 100 μm × 20 μm after deposition on the substrates. The detailed transfer method can be found in Ref. [16]. All the PDMS substrates were 40 mm in length, 10 mm in width, and 1 mm in thickness.

Using a loading device combined with a Raman spectroscopy system, we conducted the uniaxial tensile tests while measuring the strain distribution of the graphene film, as schematically shown in Fig. 1(a). To be more specific, the strain of the PDMS substrate was gradually increased from 0% to 4.5% with a loading step of 0.75%. It is well known that, when graphene is strained, the frequency of its Raman 2D-peak will shift linearly [17, 18]. Therefore, by measuring the frequency shift in the Raman 2D-peak, one can directly calculate the strain of graphene if the conversion factor, i.e., Raman 2D-peak position shift rate per strain coefficient (RSS_{2D}), is known. In the experiment, we used the value of RSS_{2D} (–30.9 cm^{-1}/%)

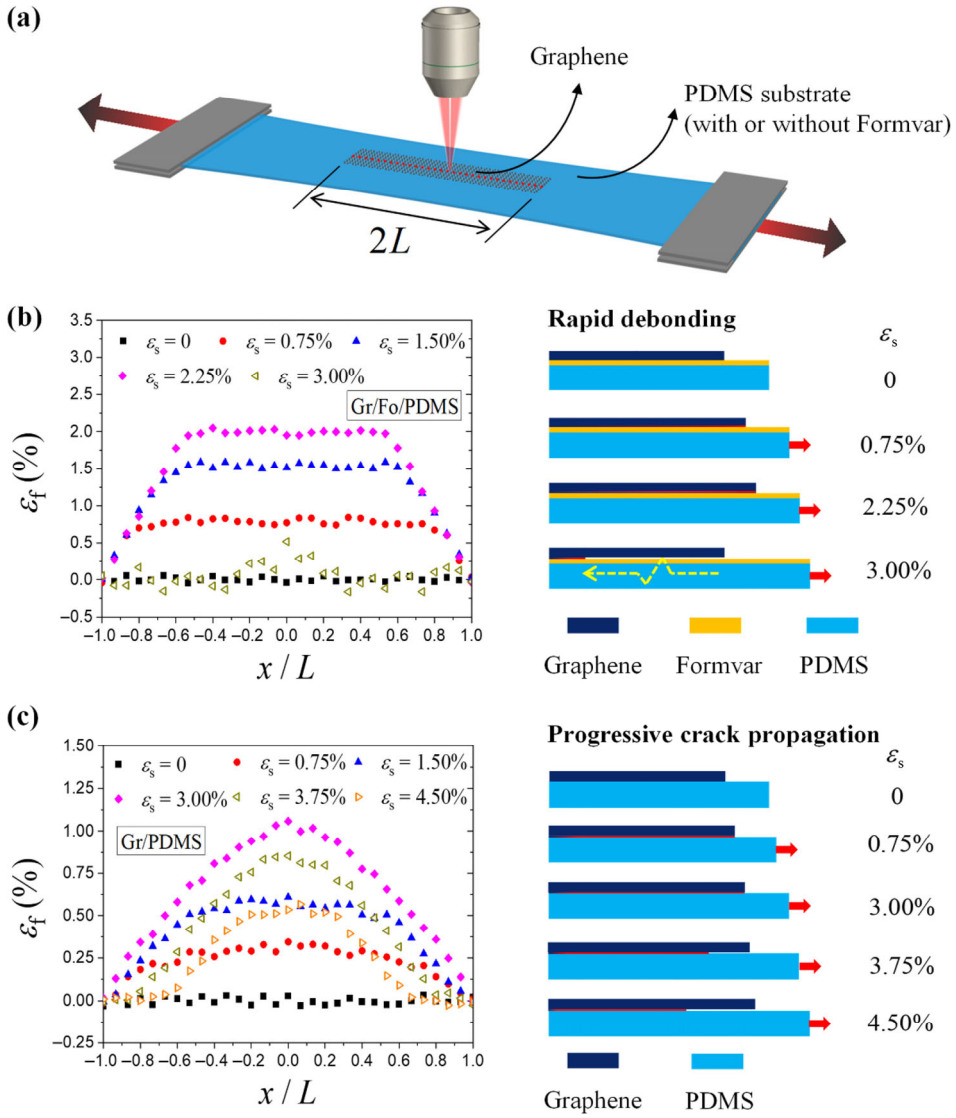

Fig. 1 (a) Schematic of the uniaxial tensile tests on graphene/formvar–PDMS and graphene/PDMS samples using a Raman spectoscopy system (the PDMS substrate and graphene are not drawn to scale; the red dashed line illustrates the sampling points along the graphene surface). (b) (left) Distributions of graphene strain of the graphene/formvar/PDMS sample under substrate strain of 0%–3.00%. (right) Schematic of the rapid debonding process of the graphene/formvar interface. (c) (left) Distributions of graphene strain of the graphene/PDMS sample under substrate strain of 0%–4.50%. (right) Schematic of the progressive crack propagation process of the graphene/PDMS interface. Red lines represent the slipped regions of the interface, and the degree of redness means the extent of sliding.

obtained on a similar system [16] to estimate the graphene strain. The Raman spectra were obtained using a Renishaw InVia system with a 633-nm He–Ne laser as the excitation source. The spot size of the laser was about 1 μm in diameter, after being focused through a 50× objective lens (numerical aperture = 0.75). A low laser power of 0.85 mW was used to avoid local heating effect or damage to the graphene film. The total number of sampling points for measuring the strain distribution along the centerline of the graphene was 31.

Figures 1(b) and 1(c) show the distributions of graphene strain of the Gr/Fo–PDMS and Gr/PDMS samples along the tensile direction at various loading stages. For the Gr/Fo–PDMS system, upon the initial stretching (0%–2.25%), the graphene strain increases almost linearly from the edge to the center, until it reaches the substrate strain in the middle part, as shown on the left side of Fig. 1(b). This strain distribution suggests that interface slip occurs from the edge of the interface and there exists approximately constant shear stress in the slipped region, as schematically depicted by the red lines along the interface in the right panel of Fig. 1(b). Despite the slipped region, the interface in the middle part remains almost intact during the initial stretching. However, when the substrate strain is further increased to 3.00%, the graphene strain across the sample suddenly drops to nearly zero, except for a narrow region with very small tensile strain at the center. Though direct observation of the graphene/polymer interface during debonding is challenging, the strain distribution indicates that complete debonding has occurred in most areas of the Gr/Fo–PDMS interface and only a small region at the center remains bonded but has also slipped. The rapid debonding process is schematically illustrated in the right panel of Fig. 1(b).

In contrast, for the Gr/PDMS system, the strain of graphene keeps increasing non-linearly from the edge to the center upon initial stretching and no constant strain region can be observed, as shown by the left panel of Fig. 1(c). It is worth noting that the maximum strain of graphene still occurs at the center but its magnitude is always significantly lower than the applied strain of the substrate. For example, when the substrate strain is 3.00%, the maximum strain of graphene is only 1.00%. This non-linear strain distribution implies that the entire interface has fully slipped even under small substrate strain, as illustrated by the right panel of Fig. 1(c). The graphene strain gradually evolves and becomes larger when the substrate strain is increased from 0 to 3.00%. When the substrate strain is beyond 3.00%, the overall graphene strain decreases and a zero-strain region starts to appear from the free edge of the interface. Upon further stretching, the zero-strain region expands gradually from the edge to the center. This suggests that the interface has fully bedonded from the edge but the decohesion occurs much more progressively unlike the case of Gr/Fo–PDMS system.

The above experimental results show that the interface decohesion can occur in distinct fashions depending on the nature of the interfacial adhesion: one is through rapid debonding and the other is via more progressive crack propagation. In the following, we will propose a theoretical decohesion model to reveal the mechanism underlying the distinct failure behavior and identify the key governing factors.

3 Theoretical model and discussions

To better understand the decohesion process of the graphene/substrate interface due to uniaxial stretch, a mechanics model was considered. As shown in Fig. 2(a), an elastic thin film with thickness h and length L is originally bonded to an elastic substrate and then the substrate is gradually stretched along the lateral direction to initiate decohesion of the thin film. The adhesive interaction between the film and the substrate follows a shear cohesive zone model, consisting of a strengthening stage, a full frictional slip stage, and a debonded stage, as depicted in Fig. 2(b). During the strengthening state with partial slip, the interfacial shear stress, τ, increases linearly with the slip distance, δ, until it reaches a maximum shear strength, τ_{m}, at the initial strengthening slip distance, δ_{i}. As the slip continues, the interface enters the full frictional slip stage, where the shear stress stays constant at τ_{m} for $\delta_{\mathrm{i}} \le \delta \le \delta_{\mathrm{c}}$. When the slip distance becomes larger than a final critical distance, δ_{c}, the interfacial shear stress drops to zero suddenly, representing a fully debonded state. Compared with the cohesive zone models adopted in previous works

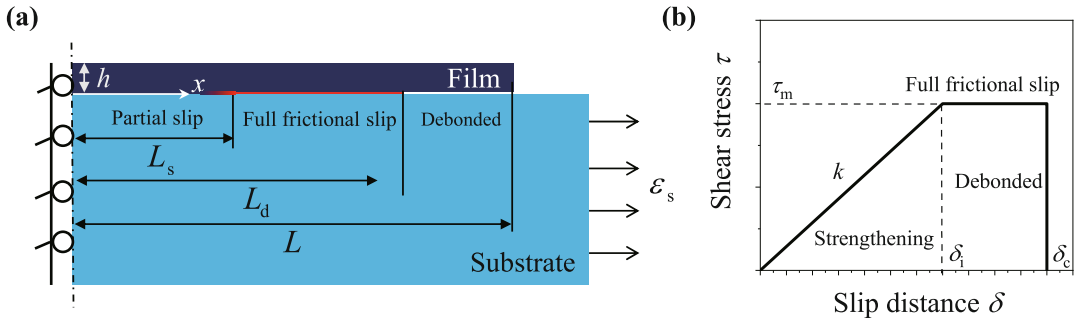

Fig. 2 (a) A two-dimensional model for decohesion of an elastic thin film from a stretched substrate; only half of the system is considered due to symmetry. (b) Cohesive zone model depicts the shear interaction of the adhesive interface.

[12–14], our model considers both a constant shear strength τ_m and a finite final slip distance δ_c, which is essential to describe the full debonding behavior. Here, we can define a dimensionless parameter $\lambda=(\delta_c-\delta_i)/\delta_i$ to describe the relative slip length between the full frictional slip stage and the initial strengthening stage. For $\lambda>0$, the cohesive zone has a trapezoidal shape and it reduces to a triangular shape for $\lambda=0$. Corresponding to the different interfacial states, the film/substrate interface can be divided into three regions: the strengthening/partial slip region at $0\le x\le L_s$, the full frictional slip region at $L_s\le x\le L_d$ and the debonded region at $L_d\le x\le L$. Based on the assumption of the modified shear lag model, the graphene strain will reduce to zero linearly in the full frictional slip region, which agrees with our experimental results shown in Figs. 1(b) and 1(c). If the shear stress instead drops to zero within a certain slip distance, one would expect a nonlinear graphene strain distribution between the full frictional slip region and debonded region, which is not evident in our experiment.

Since the thickness of graphene is much smaller than that of the substrate, it is assumed that the existence of the film will not affect the deformation of the substrate. Therefore, the strain of the substrate, ε_s, is uniform and the displacement of the substrate, u_s, can be written as

$$u_s=\varepsilon_s\cdot x \tag{1}$$

The tensile strain is transferred to the film through the interfacial shear stress. The stress, σ_f, and strain, ε_f, of the film along the x-direction satisfy the constitutive equation in Eq. (2):

$$\sigma_f=E_f\varepsilon_f \tag{2}$$

where E_f is the elastic modulus of the film and ε_f can be further written as a function of the displacement of the film, u_f,

$$\varepsilon_f=\frac{\mathrm{d}u_f}{\mathrm{d}x} \tag{3}$$

In the meantime, the interfacial slip distance can be calculated by finding the displacement difference between the film and the substrate:

$$\delta=u_s-u_f \tag{4}$$

Considering the equilibrium of the film, one can calculate the interfacial shear stress, τ, along the x-direction as

$$\tau=-h\frac{\mathrm{d}\sigma_f}{\mathrm{d}x} \tag{5}$$

According to the cohesive zone model given in Fig. 2(b), the relationship between interfacial shear stress and slip distance follows

$$\tau=\begin{cases}k\delta & ,0\le\delta\le\delta_i\\ \tau_m & ,\delta_i\le\delta\le\delta_c\\ 0 & ,\delta\ge\delta_c\end{cases} \tag{6}$$

Substituting Eqs. (1)–(5) into Eq. (6), one can obtain the governing equations of the system in terms of u_f

$$hE_f\frac{\mathrm{d}^2u_f}{\mathrm{d}x^2}=\begin{cases}k(u_f-\varepsilon_s\cdot x) & ,0\le x\le L_s\\ -\tau_m & ,L_s\le x\le L_d\\ 0 & ,L_d<x\le L\end{cases} \tag{7}$$

and the corresponding boundary conditions are

$$u_{\mathrm{f}}\big|_{x=0}=0 \tag{8}$$

$$\frac{\mathrm{d}u_{\mathrm{f}}}{\mathrm{d}x}\bigg|_{x=L_{\mathrm{d}}}=0 \tag{9}$$

According to the definitions of L_{s} and L_{d}, we have

$$\delta\big|_{x=L_{\mathrm{s}}}=\delta_{\mathrm{i}} \tag{10}$$

$$\delta\big|_{x=L_{\mathrm{d}}}=\delta_{\mathrm{c}} \tag{11}$$

By solving Eqs. (7)–(11), solution of u_{f} can be obtained and the strain of the film can be calculated subsequently by Eq. (3). It is worth noting that this theoretical model is not only suitable for 2D material/substrate systems, but also generally applicable to any thin film/substrate system when the thickness of film is far less than that of the substrate.

To illustrate the essential decohesion behavior without adding too much complicity, we will first discuss the case of $\lambda=0$, where the cohesive zone model has a triangular shape without the full frictional slip stage. In this case, one has $\delta_{\mathrm{c}}=\delta_{\mathrm{i}}$ and $L_{\mathrm{s}}=L_{\mathrm{d}}$. By solving Eq. (7) and invoking Eqs. (8) and (9), for any given substrate strain ε_{s}, we can get the strain distribution of the film:

$$\varepsilon_{\mathrm{f}}(x)=\begin{cases}\varepsilon_{\mathrm{s}}\cdot\left(1-\dfrac{\cosh\left(x/l_0\right)}{\cosh\left(L_{\mathrm{s}}/l_0\right)}\right), & 0\le x\le L_{\mathrm{s}}\\ 0, & L_{\mathrm{s}}<x\le L\end{cases} \tag{12}$$

and the interfacial shear stress distribution:

$$\tau(x)=\begin{cases}\tau_{\mathrm{m}}\dfrac{\varepsilon_{\mathrm{s}}}{\varepsilon_0}\dfrac{\sinh\left(x/l_0\right)}{\cosh\left(L_{\mathrm{s}}/l_0\right)}, & 0\le x\le L_{\mathrm{s}}\\ 0, & L_{\mathrm{s}}<x\le L\end{cases} \tag{13}$$

where $l_0=\sqrt{\dfrac{E_{\mathrm{f}}h\delta_{\mathrm{i}}}{\tau_{\mathrm{m}}}}$, $\varepsilon_0=\sqrt{\dfrac{\tau_{\mathrm{m}}\delta_{\mathrm{i}}}{E_{\mathrm{f}}h}}$ are the characteristic length and strain. The length of the partial slip region L_{s}, i.e., the length of the interface that remains bonded, can be determined by Eq. (10) and Eq. (6), which gives

$$L_{\mathrm{s}}=\begin{cases}\dfrac{l_0}{2}\ln\left(\dfrac{\varepsilon_{\mathrm{s}}/\varepsilon_0+1}{\varepsilon_{\mathrm{s}}/\varepsilon_0-1}\right), & \varepsilon_{\mathrm{s}}\ge\varepsilon_{\mathrm{s}}^{\mathrm{i}}\\ L, & \varepsilon_{\mathrm{s}}<\varepsilon_{\mathrm{s}}^{\mathrm{i}}\end{cases} \tag{14}$$

where $\varepsilon_{\mathrm{s}}^{\mathrm{i}}$ is the initial critical debonding strain given by

$$\varepsilon_{\mathrm{s}}^{\mathrm{i}}=\varepsilon_0\cdot\coth\left(L/l_0\right) \tag{15}$$

Figure 3(a) shows the variation of the relative length of the bonded region, L_{s}/L, with the substrate strain ε_{s}. Generally, when the substrate is gradually stretched, the interface will remain intact initially and then start to get debonded at different rates after the critical strain, $\varepsilon_{\mathrm{s}}^{\mathrm{i}}$, determined by Eq. (15). Furthermore, one can see that the debonding behavior is essentially determined by a parameter, $\bar{L}=L/l_0$, which is the dimensionless length of the thin film. The dimensionless initial debonding rate can be derived from Eqs. (14) and (15) as

$$\frac{\mathrm{d}\left(L_{\mathrm{s}}/L\right)}{\mathrm{d}\left(\varepsilon_{\mathrm{s}}/\varepsilon_0\right)}\bigg|_{\varepsilon_{\mathrm{s}}=\varepsilon_{\mathrm{s}}^{\mathrm{i}}}=\frac{1}{\bar{L}\left(1-\coth^2(\bar{L})\right)} \tag{16}$$

One can see that larger $\bar{L}$ value will result in a higher decrease rate of the bonded length once the interface debonding is initiated. For example, for systems with $\bar{L}=10$, the dimensionless initial debonding rate is -1.21×10^{7} and the debonding process is rather abrupt; while, for systems with $\bar{L}=1$, the initial

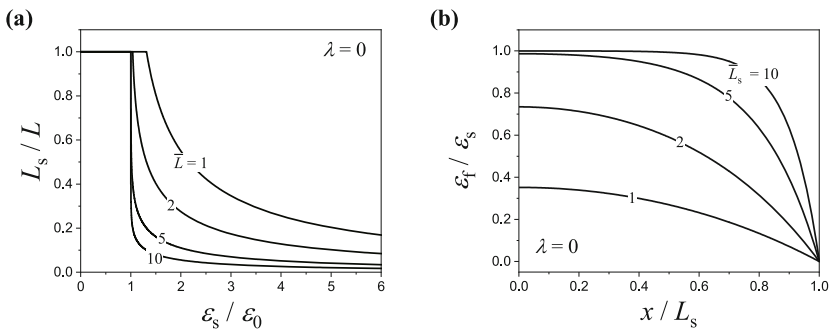

Fig. 3 (a) Variations of L_{s}/L with $\varepsilon_{\mathrm{s}}/\varepsilon_0$ for $\lambda=0$. (b) Variations of $\varepsilon_{\mathrm{f}}/\varepsilon_{\mathrm{s}}$ with x/L_{s} for $\lambda=0$.

debonding rate is −1.38 and the debonding process is much more progressive. However, despite the initial debonding rate, the debonding process would slow down and become more progressive when the length of the bonded region L_s gets close to l_0.

In order to examine the strain transfer capability of the interface, we plotted the strain distributions of the thin film along the *x*-direction for systems with different bonded lengths (i.e., different L_s values). As shown in Fig. 3(b), the strain of the film is zero at the edge of the bonded region and it increases gradually when the location moves towards the center. The maximum strain value at the center is given by Eq. (12) and notably affected by the dimensionless length of the bonded region, i.e., $\bar{L}_s = L_s / l_0$, according to Eq. (17):

$$\varepsilon_f(0) = \varepsilon_s \cdot \left(1 - \frac{1}{\cosh(\bar{L}_s)}\right) \tag{17}$$

The calculation results of Eq. (17) show that the maximum strain at the center of the film is more than 98.7% of substrate strain when $\bar{L}_s$ is larger than 5, but is less than 73.4% of substrate strain when $\bar{L}_s$ is less than 2. Therefore, the dimensionless bonded length $\bar{L}_s$ can be used to describe the strain transfer capability of the interface.

In order to better illustrate the impact of the dimensionless length $\bar{L}$ on the debonding process and compare it with the experiments, we calculated the strain distributions of the film while incrementally increasing the substrate strain for different $\bar{L}$ values. As shown in Fig. 4(a), for the system with $\bar{L} = 10$, when the substrate strain is below the initial critical debonding strain ε_s^i, the film strain at the center can catch up with the substrate strain. However, when the substrate strain is slightly above ε_s^i, the interface debonding is initiated from the free edge and propagates rapidly towards the center. For example, when the substrate strain is 1.01% (about 1.0% higher than ε_s^i), 74% of the film becomes debonded. In contrast, for the system with $\bar{L} = 1$ in Fig. 4(b), due to partial slip of the interface, the film strain at the center cannot follow the substrate strain even when the substrate strain is well below ε_s^i. Despite the relatively low strain transfer capability, the interface debonding process is much more progressive when the substrate strain is beyond ε_s^i. For example, when the substrate strain is 1.50% (15.4% higher than ε_s^i), 80% of the film is still bonded.

Based on the discussion above, the dimensionless length $\bar{L}$ of the film is an important parameter that dictates the debonding rate of the thin film/substrate system when a triangular shear cohesive zone model is considered. However, in real graphene/polymer substrate systems, a constant frictional shear stress is often observed before the interface is completely debonded [7, 10]. In order to better capture the debonding behavior, we will consider the more realistic shear cohesive zone model with a constant shear stress during the frictional sliding stage, i.e., systems with $\lambda > 0$. In such cases, we have $\delta_c > \delta_i$ and $L_d \geq L_s$.

Analogous to the case of $\lambda = 0$, by solving Eq. (7) and invoking Eqs. (8), (9), and (10), we can obtain the strain distribution of the film:

$$\varepsilon_f(x) = \begin{cases} \varepsilon_s \cdot \left[1 - \dfrac{\cosh(x/l_0)}{(L_d/l_0 - L_s/l_0)\sinh(L_s/l_0) + \cosh(L_s/l_0)}\right], & 0 \leq x \leq L_s \\ \varepsilon_s \cdot \dfrac{L_d/l_0 - x/l_0}{(L_d/l_0 - L_s/l_0) + \coth(L_s/l_0)}, & L_s < x \leq L_d \\ 0, & L_d < x \leq L \end{cases} \tag{18}$$

The values of L_s and L_d can be determined by solving Eqs. (6), (10), and (11), which gives

$$\varepsilon_s = \varepsilon_0 \cdot \left(L_d/l_0 - L_s/l_0 + \coth(L_s/l_0)\right) \tag{19}$$

$$\varepsilon_s = \frac{\varepsilon_0}{2} \cdot \left(L_d/l_0 - L_s/l_0 + \frac{2\lambda}{L_d/l_0 - L_s/l_0}\right) \tag{20}$$

It is noted that, for a physically meaningful system, we have $L_s \leq L_d \leq L$. Therefore, the determination of L_s and L_d should be treated more carefully. When the substrate strain ε_s is smaller than ε_s^i, the whole interface has not yet entered the full frictional slip stage, which requires $L_s = L_d = L$. Therefore, ε_s^i can be determined from Eq. (19) by letting $L_s = L_d = L$, which is equivalent to Eq. (15). When the substrate strain ε_s is larger than ε_s^i but smaller than another critical strain ε_s^c, full frictional slip zone starts to emerge from the edge but still no debonding has occurred. In this case, we have $L_d = L$ and the values

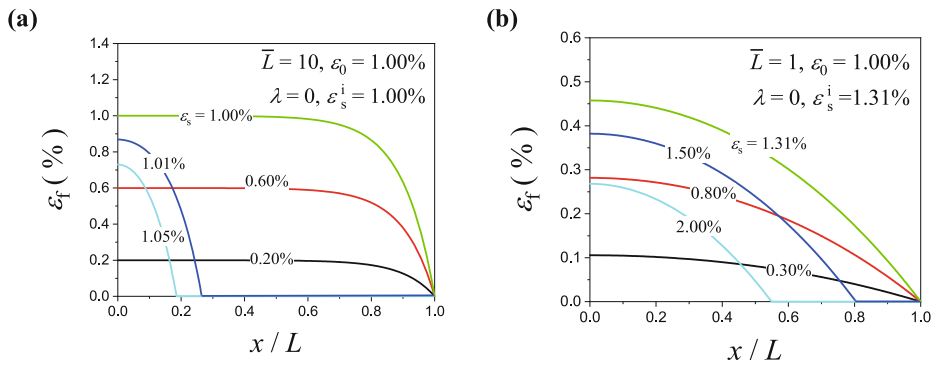

Fig. 4 Distributions of the film strain along the x-direction for (a) $\bar{L}=10$ and (b) $\bar{L}=1$.

of L_s can be determined from Eq. (19). Finally, when the substrate strain is larger than ε_s^c, L_s and L_d can be determined by simultaneously solving Eqs. (19) and (20):

$$L_s=\frac{l_0}{2}\ln\left(\frac{\sqrt{(\varepsilon_s/\varepsilon_0)^2-2\lambda}+1}{\sqrt{(\varepsilon_s/\varepsilon_0)^2-2\lambda}-1}\right) \tag{21}$$

$$L_d=l_0\left[\frac{1}{2}\ln\left(\frac{\sqrt{(\varepsilon_s/\varepsilon_0)^2-2\lambda}+1}{\sqrt{(\varepsilon_s/\varepsilon_0)^2-2\lambda}-1}\right)+\varepsilon_s/\varepsilon_0-\sqrt{(\varepsilon_s/\varepsilon_0)^2-2\lambda}\right] \tag{22}$$

Based on Eq. (22), one can determine ε_s^c by letting $L_d=L$, $\varepsilon_s=\varepsilon_s^c$ and solving Eq. (23):

$$L=l_0\left[\frac{1}{2}\ln\left(\frac{\sqrt{(\varepsilon_s^c/\varepsilon_0)^2-2\lambda}+1}{\sqrt{(\varepsilon_s^c/\varepsilon_0)^2-2\lambda}-1}\right)+\varepsilon_s^c/\varepsilon_0-\sqrt{(\varepsilon_s^c/\varepsilon_0)^2-2\lambda}\right] \tag{23}$$

Figure 5 shows the variations of the relative bonded length L_d/L with the substrate strain ε_s for different $\bar{L}$ values when $\lambda=1$ and $\lambda=10$. Comparing Figs. 5(a) and 5(b) with Fig. 3(a), one can see that introduction of the full frictional slip stage can toughen the interface and postpone the occurrence of the debonding process. However, the debonding rate once a crack is initiated from the free edge is still determined by the value of $\bar{L}$, i.e., larger $\bar{L}$ leads to more rapid debonding for both $\lambda=1$ and $\lambda=10$.

In order to analyze the strain transfer capability of different interface systems with $\lambda=1$ and $\lambda=10$, we plotted the strain distributions of the film along the x-direction for systems with different partial slip lengths. As shown in Figs. 6(a) and 6(b), the strain of the film increases linearly from the edge towards the center due to the existence of the full frictional slip region within $L_s\le x\le L_d$. Then the film strain levels off gradually within the partial slip/strengthening zone $0\le x\le L_s$. For both cases of $\lambda=0$ and $\lambda>0$, the maximum strain at the center of the film is given by Eq. (18), i.e.,

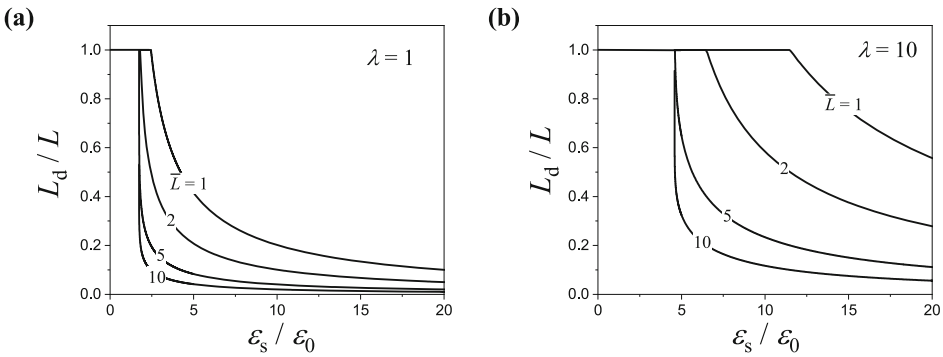

Fig. 5 Variations of L_d/L with $\varepsilon_s/\varepsilon_0$ for (a) $\lambda=1$ and (b) $\lambda=10$.

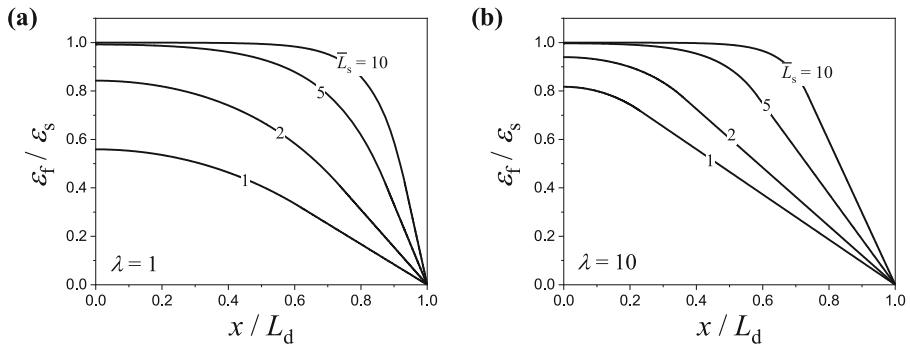

Fig. 6 Variations of $\varepsilon_f/\varepsilon_s$ with x/L_d for (a) $\lambda=1$ and (b) $\lambda=10$.

$$\varepsilon_f(0)=\varepsilon_s\cdot\left(1-\frac{1}{\sqrt{2\lambda\cdot\sinh^2(\bar{L}_s)+\cosh^2(\bar{L}_s)}}\right) \tag{24}$$

which is affected by dimensionless length $\bar{L}_s$ and λ. For $\lambda=1$ and $\lambda=10$, the central strain is close to the substrate strain when $\bar{L}_s$ is larger than 5, but is less than the substrate strain when $\bar{L}_s$ is smaller than 2. Moreover, with the increase of λ, the distribution curve of film strain tends to ascend overall for fixed $\bar{L}_s$, which means the larger frictional sliding zone will strengthen the strain transfer capability of the adhesive interface. For large values of $\bar{L}_s$, i.e., 5 and 10, the strengthening effect is limited, but for smaller values of $\bar{L}_s$, i.e., 2 and 1, the strengthening effect is quite high.

To better compare the theoretical results with the experiments, we calculated the strain distributions of the film while incrementally increasing the substrate strain for different values of $\bar{L}$ and λ. As shown in Figs. 7(a) and 7(b), for the systems with $\bar{L}=10$ and $\lambda=1$ or 10, the critical substrate strain to initiate debonding is enhanced when compared with the results of $\lambda=0$ shown in Fig. 4(a). Because of the existence of the frictional slip stage, the critical debonding strain is increased from $\varepsilon_s^i=1.00\%$ for

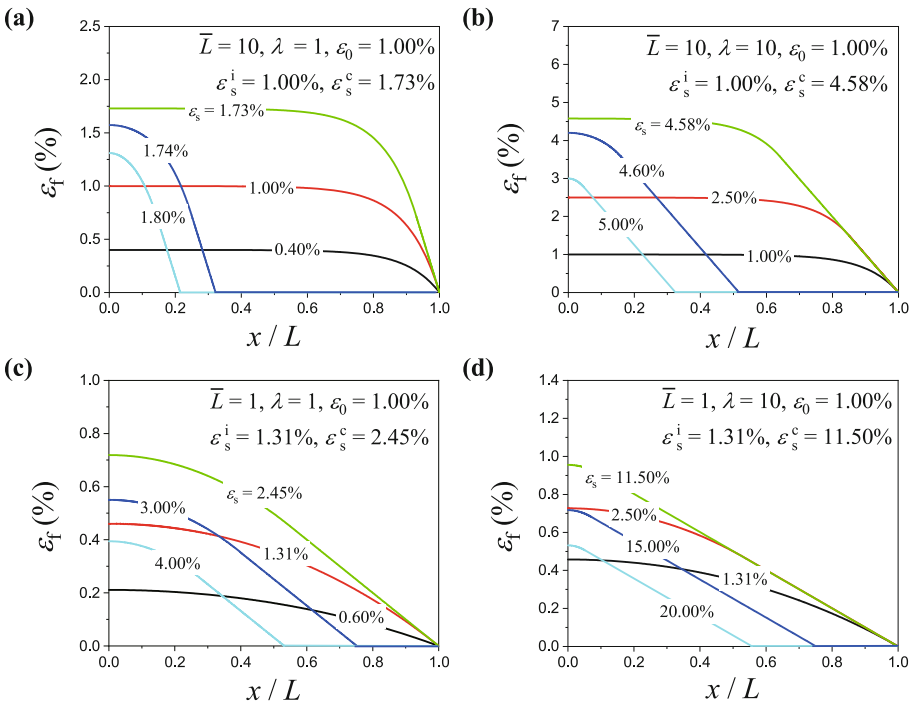

Fig. 7 Distribution of film strain along x-direction for rapid debonding: (a) $\bar{L}=10$, $\lambda=1$ and (b) $\bar{L}=10$, $\lambda=10$; or progressive crack propagation: (c) $\bar{L}=1$, $\lambda=1$ and (d) $\bar{L}=1$, $\lambda=10$ of the adhesive interface.

$\lambda = 0$, to $\varepsilon_s^c = 1.73\%$ for $\lambda = 1$, and to $\varepsilon_s^c = 4.58\%$ for $\lambda = 10$. Regardless of the values of λ, for the systems with $\bar{L} = 10$, the interfacial debonding rate is very high once a crack is initiated ($\varepsilon_s \geq \varepsilon_s^c$). In contrast, Figs. 7(c) and 7(d) show the calculation results for the systems with $\bar{L} = 1$ and $\lambda = 1$ or 10. Again, the critical debonding strain for $\lambda > 0$ is enhanced when compared with the case of $\lambda = 0$, as shown in Fig. 4(b). However, for the systems with $\bar{L} = 1$, the debonding process is much more progressive compared with the cases with $\bar{L} = 10$ regardless of the values of λ.

Based on the model analysis, the critical substrate strain to initiate debonding is governed by three dimensionless parameters, i.e., $\bar{L}$, λ, and ε_0. However, the debonding rate is mainly dependent on $\bar{L}$. The distinct decohesion behaviors observed in the experiments suggest that the two samples may have drastically different system parameters, which are determined by the properties of the interfacial adhesion. Since the thickness $h = 0.34$ nm and the original bonded length $L = 50$ um of the graphene films are known and the effective modulus of grapheme E_f is 1 TPa [19], by setting interfacial parameters k, τ_{max}, and λ as fitting parameters, we can fit the experimental data using Eqs. (18), (21), and (22). After k, τ_{max}, and λ are obtained, we can further calculate $\bar{L}$ and ε_0.

The fitting curves are shown in Fig. 8 and the corresponding fitted parameters are listed in Table 1. As one can see, the fitting curves show good consistency with the experimental data. According to the fitting results, the shear strength τ_{max} and the relative length of full friction slip stage λ of the Gr/Fo/PDMS interface are much larger than those of the Gr/PDMS interface. These values are reasonable and expected, because the formvar layer was known to be beneficial for strengthening interfacial adhesion between graphene and PDMS [16, 20]. The stronger adhesion with formvar is attributed to the liquid–solid phase transition for achieving conformal interfacial contact and the appropriate value of the Poisson's ratio to avoid potential buckling of graphene along the transverse direction during substrate stretching [20]. Because of the difference in interfacial adhesion properties, the dimensionless length of the Gr/Fo/PDMS interface ($\bar{L} = 12$) is much larger than that of the Gr/PDMS interface ($\bar{L} = 1.2$). Therefore, the debonding process is much rapider for the Gr/Fo/PDMS interface. It is worth noting that no failure of polycrystalline graphene at the grain boundaries was observed in our experiments; otherwise the in-plane strain of graphene near the crack edge would drop substantially. This was reasonable since the graphene/polymer interface was relatively weak compared with the strength of polycrystalline graphene.

4 Conclusions

The decohesion behavior of graphene films from uniaxially-stretched PDMS substrates with different interfacial adhesion properties is characterized experimentally. Two drastically different decohesion rates, i.e., rapid debonding and progressive crack propagation, are observed depending on the nature of the adhesive interface. To unveil the mechanism underlying the distinct decohesion processes, an improved shear-lag model with trapezoidal cohesive

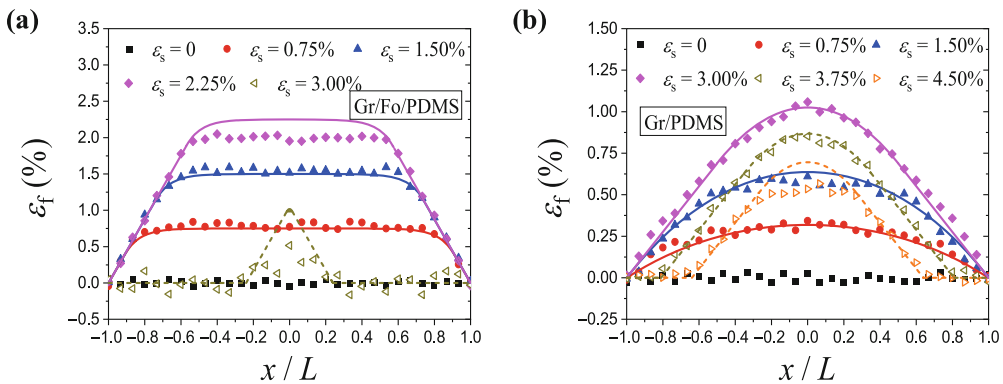

Fig. 8 Distribution of the film strain for (a) Gr/Fo/PDMS interface and (b) Gr/PDMS interface under different applied substrate strains. The solid curves are fitted using Eqs. (18), (21), and (22).

Table 1 Fitted interfacial parameters of the cohesive zone model for both Gr/Fo/PDMS and Gr/PDMS interfaces.

Interfacial parameter	Gr/Fo/PDMS interface	Gr/PDMS interface
k (TPa/m)	19.6	0.177
τ_{max} (kPa)	291	91.4
λ	19.2	1.52

zone interaction has been proposed. The theoretical model shows that the critical substrate strain required to initiate debonding process is governed by three dimensionless parameters, i.e., $\bar{L}$, λ, and ε_0. While the propagation rate of the interface crack after debonding is primarily determined by the dimensionless length $\bar{L}$. For systems with larger values of $\bar{L}$, debonding of the interface will occur at a higher rate once initiated. Finally, the experimental data are fitted by the theoretical model to extract the intrinsic adhesion properties of different interfaces. Our work provides a general theoretical tool for understanding and optimizing the mechanical properties of thin film/substrate structures with frictional adhesive interfaces.

Acknowledgements

We gratefully acknowledge the support from the National Natural Science Foundation of China (Nos. 12025203, 11921002, and 11890671), the National Key R&D Program of China (No. 2022YFF0706100), and the Initiative Program of State Key Laboratory of Tribology in Advanced Equipment (No. SKLT2022A01). We thank Dr. Changyi Hong (Tianjin University) for preparing the graphene/PDMS and graphene/formvar–PDMS samples used in the experiments.

Declaration of competing interest

The authors have no competing interests to declare that are relevant to the content of this article.

References

[1] Zhang S, Ma T B, Erdemir A, Li Q Y. Tribology of two-dimensional materials: From mechanisms to modulating strategies. *Mater Today* **26**: 67–86 (2019)

[2] Kim S J, Choi K, Lee B, Kim Y, Hong B H. Materials for flexible, stretchable electronics: Graphene and 2D materials. *Annu Rev Mater Res* **45**: 63–84 (2015)

[3] Kanahashi K, Pu J A, Takenobu T. 2D materials for large-area flexible thermoelectric devices. *Adv Energy Mater* **10**(11): 1902842 (2020)

[4] Glavin N R, Chabak K D, Heller E R, Moore E A, Prusnick T A, Maruyama B, Walker D E Jr, Dorsey D L, Paduano Q, Snure M. Flexible gallium nitride for high-performance, strainable radio-frequency devices. *Adv Mater* **29**(47): 1701838 (2017)

[5] Gong L, Kinloch I A, Young R J, Riaz I, Jalil R, Novoselov K S. Interfacial stress transfer in a graphene monolayer nanocomposite. *Adv Mater* **22**(24): 2694–2697 (2010)

[6] Anagnostopoulos G, Androulidakis C, Koukaras E N, Tsoukleri G, Polyzos I, Parthenios J, Papagelis K, Galiotis C. Stress transfer mechanisms at the submicron level for graphene/polymer systems. *ACS Appl Mater Interfaces* **7**(7): 4216–4223 (2015)

[7] Xu C C, Xue T, Guo J G, Kang Y L, Qiu W, Song H B, Xie H M. An experimental investigation on the tangential interfacial properties of graphene: Size effect. *Mater Lett* **161**: 755–758 (2015)

[8] Xu C C, Xue T, Guo J G, Qin Q H, Wu S, Song H B, Xie H M. An experimental investigation on the mechanical properties of the interface between large-sized graphene and a flexible substrate. *J Appl Phys* **117**(16): 164301 (2015)

[9] Wang G R, Dai Z H, Liu L Q, Hu H, Dai Q, Zhang Z. Tuning the interfacial mechanical behaviors of monolayer graphene/PMMA nanocomposites. *ACS Appl Mater Interfaces* **8**(34): 22554–22562 (2016)

[10] Xu C C, Xue T, Qiu W, Kang Y L. Size effect of the interfacial mechanical behavior of graphene on a stretchable substrate. *ACS Appl Mater Interfaces* **8**(40): 27099–27106 (2016)
[11] Erdem Alaca B, Saif M T A, Sehitoglu H. On the interface debond at the edge of a thin film on a thick substrate. *Acta Mater* **50**(5): 1197–1209 (2002)
[12] Jiang T, Huang R, Zhu Y. Interfacial sliding and buckling of monolayer graphene on a stretchable substrate. *Adv Funct Mater* **24**(3): 396–402 (2014)
[13] Guo G D, Zhu Y. Cohesive-shear-lag modeling of interfacial stress transfer between a monolayer graphene and a polymer substrate. *J Appl Mech* **82**(3): 031005 (2015)
[14] Dai Z H, Wang G R, Liu L Q, Hou Y, Wei Y G, Zhang Z. Mechanical behavior and properties of hydrogen bonded graphene/polymer nano-interfaces. *Compos Sci Technol* **136**: 1–9 (2016)
[15] Cui T, Yip K, Hassan A, Wang G R, Liu X J, Sun Y, Filleter T. Graphene fatigue through van der Waals interactions. *Sci Adv* **6**(42): eabb1335 (2020)
[16] Wang Y L, Wang Y, Xu C, Zhang X W, Mei L, Wang M, Xia Y, Zhao P, Wang H T. Domain-boundary independency of Raman spectra for strained graphene at strong interfaces. *Carbon* **134**: 37–42 (2018)
[17] Mohiuddin T M G, Lombardo A, Nair R R, Bonetti A, Savini G, Jalil R, Bonini N, Basko D M, Galiotis C, Marzari N, *et al*. Uniaxial strain in graphene by Raman spectroscopy: G peak splitting, Grüneisen parameters, and sample orientation. *Phys Rev B* **79**(20): 205433 (2009)
[18] Tsoukleri G, Parthenios J, Papagelis K, Jalil R, Ferrari A C, Geim A K, Novoselov K S, Galiotis C. Subjecting a graphene monolayer to tension and compression. *Small* **5**(21): 2397–2402 (2009)
[19] Shen C, Oyadiji S O. The processing and analysis of graphene and the strength enhancement effect of graphene-based filler materials: A review. *Mater Today Phys* **15**: 100257 (2020)
[20] Jin Y, Ren Q, Liu J, Zhang Y, Zheng H, Zhao P. Stretching graphene to 3.3% strain using formvar-reinforced flexible substrate. *Exp Mech* **62**(5): 761–767 (2022)

Bo PENG. He is a senior engineer in Huawei Technologies Co., Ltd. He received his Ph.D. degree in engineering mechanics in 2021 from Tsinghua University, Beijng, China and B.E. degree in aircraft design in 2016 from Beihang University, Beijng, China. His current research aims at the theoretical analysis and experimental characterization of solid adhesive contact interfaces.

Qunyang LI. He is a professor in the Department of Engineering Mechanics at Tsinghua University. Before taking this position, he worked as a postdoctoral researcher and research scientist at the University of Pennsylvania, Philadelphia, USA from 2008 to 2012. He received his Ph.D. degree from the Brown University, Providence, USA in 2008 and B.S. and M.S. degrees in engineering mechanics from Tsinghua University in 2001 and 2003, respectively. His current research aims at understanding how surfaces interact at small scales and bridging nanoscale intrinsic properties to macroscale behaviors through experiments and mechanics modeling.